Structural Polymorphism of Telomere DNA: Interquadruplex and Duplex–Quadruplex Conversions Probed by Raman Spectroscopy†

Takashi Miura‡ and George J. Thomas, Jr.*

Division of Cell Biology and Biophysics, School of Biological Sciences, University of Missouri, Kansas City, Missouri 64110-2499

Received February 16, 1994; Revised Manuscript Received May 4, 1994®

ABSTRACT: The solution secondary structures and nucleotide conformations in the telomeric DNA of *Oxytricha nova* have been determined by Raman spectroscopy. Structural polymorphism is demonstrated for both single-stranded [$d(T_4G_4)_4$] and double-stranded [$d(G_4T_4G_4)\cdot d(C_4A_4C_4)$] telomere models. In the case of $d(T_4G_4)_4$, which is a prototype for the single-stranded telomeric tail, an interquadruplex equilibrium involving parallel and antiparallel strand configurations is shown to be governed by the solution concentrations of both Na^+ and K^+. In both the parallel and antiparallel quadruplexes of $d(T_4G_4)_4$, the local geometry of the phosphodiester backbone is similar to that of canonical B DNA, and associations between bases of the guanine quartet involve Hoogsteen hydrogen bonding. However, the deoxyguanosine (dG) sugar conformations are significantly different in the two quadruplexes. In the extended parallel form, dG residues assume only the C2′-*endo/anti* conformation with respect to deoxyribose pucker and glycosyl orientation. In the foldback antiparallel form, dG residues are distributed equally between C2′-*endo/anti* and C2′-*endo/syn* conformations. In the case of $d(G_4T_4G_4)\cdot d(C_4A_4C_4)$, which serves as a model for the double-stranded B DNA regions of *Oxytricha* telomeres, we show that disproportionation of the B form duplex to yield stable parallel quadruplexes of the guanine-rich strand occurs reversibly at high solution concentrations of either Na^+ or K^+. The present study reveals that both interquadruplex and duplex–quadruplex conversions of *Oxytricha* telomeric DNA are under the control of an alkali cation switch. The critical transition region encompasses cation concentrations ($[Na^+] + [K^+] \approx 150$ mM) which approximate those *in vivo*, implying biological significance for the observed structural polymorphism. We propose a molecular mechanism for the telomeric DNA transitions which is based upon the present spectroscopic results and is consistent with the concept of different affinities of Na^+ and K^+ for the central cavity of the guanine quartet. The present results also indicate how antiparallel and parallel quadruplexes may be exploited in the control of interchromosomal associations during meiotic and mitotic cell division cycles.

Telomeres, the termini of linear eukaryotic chromosomes, are essential for complete replication of chromosomal DNA (Blackburn & Szostak, 1984). Tandem repeats of simple guanine-rich sequences have been identified as the essential elements of telomeric DNA in several organisms, including *Oxytricha nova* [$d(T_4G_4)$], *Tetrahymena thermophila* [$d(T_2G_4)$], and mammals [$d(T_2AG_3)$]. In each case, the telomeric repeat extends beyond the 5′ end of its complementary strand by about 12–16 nucleotides (Klobutcher et al., 1981; Henderson & Blackburn, 1989). The resulting single-stranded overhang, or telomere tail, is capable of complex intrastrand associations (Sundquist, 1991). The typical configuration, which is stabilized by the presence of alkali metal ions, is an antiparallel quadruplex structure consisting of two interleaved hairpins (Sundquist & Klug, 1989; Williamson et al., 1989). In the case of the *Oxytricha* repeat, the antiparallel quadruplex has been shown by X-ray crystallography (Kang et al., 1992) and NMR spectroscopy (Smith & Feigon, 1992) to consist of planar guanine quartets linked by Hoogsteen 1N—H···2O and 2N—H···7N hydrogen bonding. Circular dichroism (CD)[1] studies confirm the role of the intervening dT_n loops in facilitating formation of the foldback quadruplex structure in solution (Balagurumoorthy et al., 1992).

Guanine-rich sequences are also capable of forming parallel-stranded quadruplexes, and mechanisms for antiparallel ↔ parallel interconversions have been proposed for various telomere tails (Sen and Gilbert, 1990; Balagurumoorthy et al., 1992; Chen, 1992). Typically, the interquadruplex equilibrium is sensitive to the type of alkali metal cation present in solution.

Although the biological relevance of structural polymorphism in the telomere tail is not well understood, cytological studies indicate a direct involvement of the telomere domain in interchromosome association (Wagenaar, 1969; Ashley & Wagenaar, 1974; Diaz & Lewis, 1975). Even in interphase, eukaryotic chromosomes are not distributed randomly through the nucleus. Typically, the telomeres of homologous chromosomes are associated with each other (Wagenaar, 1969). Telomere–telomere association is also observed for protein-free DNA extracted from cell nuclei (Lipps et al., 1982; Oka & Thomas, 1987) and may be mediated by association of guanine-rich regions to form a hairpin dimer (Sundquist & Klug, 1989; Williamson et al., 1989). Wagenaar (1969) has proposed that nonrandom arrangement of chromosomes, based upon telomere recognition, is a prerequisite for parallel association of homologous chromosomes (synapsis). Recently, Sen and Gilbert (1988) hypothesized that synapsis is facilitated by formation of parallel quadruplex structures at the telomeres, as well as within other guanine-rich regions of the four

† Raman Spectral Studies of Nucleic Acids. 49. Supported by NIH Grant AI18758.

* To whom correspondence may be addressed.

‡ Marion Merrell Dow Postdoctoral Fellow.

® Abstract published in *Advance ACS Abstracts,* June 15, 1994.

[1] Abbreviations: CD, circular dichroism; csOxy-1.5, $d(C_4A_4C_4)$; Oxy-1.5, $d(G_4T_4G_4)$; Oxy-4, $d(T_4G_4)_4$.

0006-2960/94/0433-7848$04.50/0

chromatids. The model of Sen and Gilbert is intriguing for its simplicity—invoking DNA polymorphism under the control of alkali ion concentration to explain the dynamic behavior of chromosomes during various stages of cell division.

We have employed Raman spectroscopy to determine the salt concentration dependence of structural polymorphism in *Oxytricha* single-stranded [$d(T_4G_4)_4$] and double-stranded [$d(G_4T_4G_4)\cdot d(C_4A_4C_4)$] telomeric sequences. The Raman spectra of these oligonucleotides in solutions containing different Na^+ and K^+ concentrations provide the first structural evidence of interquadruplex and duplex–quadruplex conversions. We have determined that both conversions can be controlled by the $[Na^+]/[K^+]$ ratio at physiological ionic strength. These results indicate that not only the single-stranded telomeric tail but also the adjoining double-stranded chromosomal region may facilitate the parallel association of chromosomes. We have determined that significant differences exist in the local conformations of nucleoside and phosphodiester residues of antiparallel and parallel telomeric structures in solution. The demonstrated polymorphism of telomeric DNA at physiological conditions supports the notion that telomeres fulfill a biological role in chromosomal rearrangements during cell division.

MATERIALS AND METHODS

1. Synthesis and Purification of Telomere DNA. The oligodeoxynucleotides, $d(T_4G_4)_4$ (Oxy-4), $d(G_4T_4G_4)$ (Oxy-1.5), and $d(C_4A_4C_4)$ (complementary strand of Oxy-1.5 or csOxy-1.5), were synthesized on an Applied Biosystems Model 381A DNA synthesizer using controlled pore glass supports and β-cyanoethyl phosphoramidite derivatives. Purification of DNA was performed on an ISCO Model 2350 HPLC system, employing a Hamilton PRP-1 (250 × 4.1 mm) reversed-phase column. The instrument was equipped with an ISCO V^4 variable-wavelength absorbance detector, a Model 2360/2361 gradient programmer, and a 250-mL injection loop and was controlled with ISCO Chemsearch chromatographic data management software. The triethylamine acetate–acetonitrile buffer was prepared using a ternary gradient in which the mobile phase contained 0.2 M triethylamine acetate (TEA-Ac) at pH 7.0, distilled water, and 99.9% acetonitrile. A flow rate of 1.0 mL/min was used. The column was heated at 90 °C to ensure elimination of DNA secondary structure during separation. The eluted peaks were monitored by UV absorbance at 297 nm. Appropriate peak fractions were pooled, frozen, and lyophilized. The purified oligonucleotides were desalted on Sephadex G-25 gel filtration columns (Pharmacia, NAP-5).

2. Sample Preparation. For preparation of the double-stranded Oxy-1.5 dodecamer, $d(G_4T_4G_4)\cdot d(C_4A_4C_4)$, equimolar amounts of Oxy-1.5 and csOxy-1.5 were mixed and annealed by heating for 15 min in a water bath thermostated at 90 °C, followed by slow cooling. Single-stranded Oxy-4 and $d(G_4T_4G_4)\cdot d(C_4A_4C_4)$ were dissolved directly in various concentrations of NaCl and KCl solutions (20–800 mM), and the pH was adjusted to 7.0 ± 0.2 by appropriate addition of NaOH or KOH. The solutions were sealed in glass capillary tubes (Kimax #34507) which could be mounted directly in the sample illuminator of the Raman spectrometer.

3. Raman Spectroscopy. Raman spectra were excited with the 514.5-nm line of an argon laser (Innova 70, Coherent Inc., Santa Clara, CA) using 250 mW of radiant power at the sample. The spectra were collected on a triple spectrograph (Triplemate Model 1877, SPEX Ind., Metuchen, NJ) equipped with a liquid nitrogen cooled, charge-coupled device detector (Model LN-CCD-1152UV, Princeton Instruments, Princeton, NJ) of 1152 × 298 pixels operating under microcomputer control. In a typical data collection protocol, three 8-min exposures were accumulated and averaged. The effective spectral slit width was 5 cm^{-1}.

Raman frequencies were calibrated using the spectrum of liquid indene. Peak positions were reproducible to within ±0.5 cm^{-1}. The frequencies cited are believed to be accurate to within ±0.5 cm^{-1} for sharp bands and ±2 cm^{-1} for broad or poorly resolved bands.

RESULTS AND INTERPRETATION

1. Nucleoside and Backbone Conformation Markers of Telomeric DNA. Telomeric DNA containing only deoxyguanosine (dG) and thymidine (dT) residues, including the Oxy-1.5 and Oxy-4 oligomers investigated here, exhibit Raman spectra which are considerably simpler than the spectra of DNA models investigated previously (reviewed in Thomas & Wang, 1988), owing to the absence of deoxyadenosine (dA) and deoxycytidine (dC) residues. We have conducted a detailed analysis of the Raman fingerprints of telomeric DNA models in both protium and deuterium substituted forms in order to reach definitive assignments for many conformationally sensitive Raman bands. The key Raman markers identified in the model compound analyses and exploited in this study are summarized in Tables 1 and 2.

2. Polymorphism of Single-Stranded Telomere DNA in Solution: Salt and Temperature Dependence of Raman Spectra of Oxy-4. a. Formation of an Antiparallel Foldback Quadruplex in 100 mM NaCl by Oxy-4. Figure 1 shows Raman spectra in the region 580–1750 cm^{-1} of Oxy-4 in 100 mM NaCl solution. The spectrum obtained at 10 °C (Figure 1, top) displays DNA phosphate marker bands at 837 and 1091 cm^{-1}, which indicate that phosphodiester (O–P–O) and phosphodioxy (PO_2^-) groups have the local geometries (Table 2) of canonical B DNA (Erfurth et al., 1972; Benevides et al., 1988). However, at these conditions the environment at guanine 7N sites in Oxy-4 is very different from that occurring in B DNA. The 1481 cm^{-1} band, which is a sensitive indicator of 7N hydrogen bonding interaction (Nishimura et al., 1985a; Benevides et al., 1991; see also Table 1), is about 9 cm^{-1} lower than the corresponding indicator in B DNA. This suggests strong hydrogen bonding to the guanine 7N acceptor sites in Oxy-4.

Additionally, a dG marker band is observed at 1324 cm^{-1} in Oxy-4 (Figure 1, top). Close examination of the Figure 1 spectrum reveals that the 1324 cm^{-1} peak is accompanied by a moderate shoulder near 1333 cm^{-1}. Previous studies have located a corresponding dG conformation marker at 1333 ± 3 cm^{-1} in B DNA, where it is diagnostic of the C2′-*endo/anti* dG conformation (Benevides et al., 1988), and at 1316 ± 2 cm^{-1} in Z DNA, where it is diagnostic of the *syn* dG conformation (Benevides et al., 1984). The occurrence of these two marker bands, as well as canonical 684 and 671 cm^{-1} markers (cf. Figure 1 and Table 1), confirms that C2′-*endo/anti* and C2′-*endo/syn* dG conformers are both present in Oxy-4. Although the Raman intensities in the Figure 1 spectrum demonstrate comparable amounts of C2′-*endo/anti* and C2′-*endo/syn* dG conformers (see also section 3, below), the present data do not discriminate between enantiomorphic pairs of alternating (*syn–anti–syn–anti*) or nonalternating (*syn–syn–anti–anti*) quartets.

These observations are entirely consistent with an antiparallel foldback quadruplex structure for Oxy-4 in 100 mM

Table 1: Conformation-Sensitive Raman Bands of Guanine Residues in Telomere DNA

Raman marker bands		structural significance in telomeric DNA complexes	
cm^{-1}	indicator[a]	structure[b]	comments
625 ± 2	C3′-*endo*/*syn* dG		not obsd in Oxy-4 or Oxy-1.5
664 ± 2	C3′-*endo*/*anti* dG		not obsd in Oxy-4 or Oxy-1.5
671 ± 2	C2′-*endo*/*syn* dG	Oxy-4 anti‖-qdpx	strong shoulder (≈50% of dG)
682 ± 3	C2′-*endo*/*anti* dG	Oxy-4 anti‖-qdpx	strong peak (≈50% of dG)
		Oxy-4 ‖-qdpx	strong peak (≈100% of dG)
		Oxy-1.5 duplex	strong peak (≈100% of dG)
		Oxy-1.5 ‖-qdpx	strong peak (≈100% of dG)
1316 ± 2	C3′-*endo*/*syn* dG		not obsd in Oxy-4 or Oxy-1.5
1318 ± 2	C3′-*endo*/*anti* dG		not obsd in Oxy-4 or Oxy-1.5
1324 ± 2	C2′-*endo*/*syn* dG	Oxy-4 anti‖-qdpx	strong peak (≈50% of dG)
1333 ± 3	C2′-*endo*/*anti* dG	Oxy-4 anti‖-qdpx	moderate shoulder
		Oxy-4 ‖-qdpx	strong peak (≈100% of dG)
		Oxy-1.5 duplex	strong peak (≈100% of dG)
		Oxy-1.5 ‖-qdpx	strong peak (≈100% of dG)
1481 ± 1	gua 7N, strong H-bond[c]	Oxy-4 anti‖-qdpx	strong peak (≈100% of dG)
		Oxy-4 ‖-qdpx	strong peak (≈100% of dG)
		Oxy-1.5 ‖-qdpx	strong peak (≈100% of dG)
1490 ± 1	gua 7N, weak H-bond[d]		not obsd in Oxy-4 or Oxy-1.5
		Oxy-1.5 duplex	strong peak (≈100% of dG)

[a] Raman indicators of dG nucleoside conformations and 7N acceptor hydrogen bonding states are reviewed in Thomas and Tsuboi (1993). See also the references cited in the text. [b] Abbreviations: ‖, parallel; anti‖, antiparallel; qdpx, quadruplex. [c] Diagnostic of Hoogsteen-type hydrogen bonding to the 7N acceptor. [d] Diagnostic of DNA structures not containing Hoogsteen-type hydrogen bonding.

Table 2: Conformation-Sensitive Raman Bands of the Phosphodiester Backbone in Telomere DNA[a]

Raman marker bands		Structural significance in telomeric DNA complexes	
cm^{-1}	indicator	structure	comments
745 ± 3	Z conformn		not obsd in Oxy-4 or Oxy-1.5
807 ± 3	A conformn		not obsd in Oxy-4 or Oxy-1.5
835 ± 7	B conformn	Oxy-4 anti‖-qdpx	strong peak at 836 cm^{-1}
		Oxy-4 ‖-qdpx	strong peak at 836 cm^{-1}
		Oxy-1.5 duplex	strong peak at 835 cm^{-1}
		Oxy-1.5 ‖-qdpx	strong peak at 833 cm^{-1}
1092 ± 1	B conformn	Oxy-4 anti‖-qdpx	strong peak
		Oxy-4 ‖-qdpx	strong peak
		Oxy-1.5 duplex	strong peak
		Oxy-1.5 ‖-qdpx	strong peak
1095 ± 2	Z conformn		not obsd in Oxy-4 or Oxy-1.5
1099 ± 1	A conformn		not obsd in Oxy-4 or Oxy-1.5

[a] Abbreviations and references as in Table 1.

NaCl solution. In this solution structure guanine–guanine hydrogen bonding utilizes the 7N acceptors (2N–H···7N), and both *syn* and *anti* glycosyl torsions are represented among the dG residues. Thus, the Raman results demonstrate for the solution structure of Oxy-4 essentially the same features revealed in the crystal structure of Oxy-1.5 (Kang et al., 1992).

b. Reversible Thermal Denaturation of the Oxy-4 Fold-back Quadruplex in 100 mM NaCl. To monitor the thermostability and reversibility of the Oxy-4 antiparallel quadruplex structure, the Raman spectrum was measured over the temperature range 10–80 °C. Representative data are shown in Figure 1. As the temperature is increased from 10 °C, major spectral changes are observed, including the following: (i) broadening of the 837 cm^{-1} phosphodiester marker, (ii) coalescence of the 671 and 684 cm^{-1} dG markers into a single band centered near 675 cm^{-1}, (iii) shift to higher frequency of the 1481 cm^{-1} Hoogsteen marker band with a simultaneous intensity increase, and (iv) shift to lower frequency of the 1579 cm^{-1} guanine band. These spectral changes, which are clearly evident in the 80 °C spectrum of Figure 1, are indicative of disordering of the DNA backbone, changes in dG nucleoside conformations, rupture of guanine–guanine hydrogen bonding, and probable alteration of guanine base stacking. These spectral and structural changes are reversible. As shown in Figure 1, the original Raman spectrum of Oxy-4 at 10 °C is recovered after the heat-denatured sample is slowly cooled.

c. Irreversible Thermal Transition of Oxy-4 in 500 mM NaCl. Figure 2 shows Raman spectra of Oxy-4 in 500 mM NaCl solution. The spectrum obtained initially at 10 °C, i.e., without heat treatment (Figure 2, top), is nearly identical to the 10 °C spectrum measured at low salt conditions (cf. Figure 1, top). This indicates that the antiparallel quadruplex structure which is formed at 10 °C in low salt solution is formed also in high salt solution. However, the effect of heating the high salt solution to 80 °C differs greatly from that reported for the low salt solution, above. The middle spectrum of Figure 2 shows that in high salt the 1481 cm^{-1} marker is unshifted with temperature, while the intensities of the 671 and 1324/1336 cm^{-1} markers are significantly altered with temperature. The Raman markers indicate that although hydrogen-bonded guanine quartets are maintained, dramatic changes occur in the conformations of deoxyguanosine residues of Oxy-4 in 500 mM NaCl. The kinetics of this structural transformation are represented by the data of Figure 3. Raman markers change gradually during the indicated 60-min period of heating at 80 °C in 500 mM NaCl. However, after 60 min, the attenuations of the 611, 671, and 1324 cm^{-1} bands and growths of the 684 and 1336 cm^{-1} bands are virtually complete. These results are interpreted in terms of a conversion

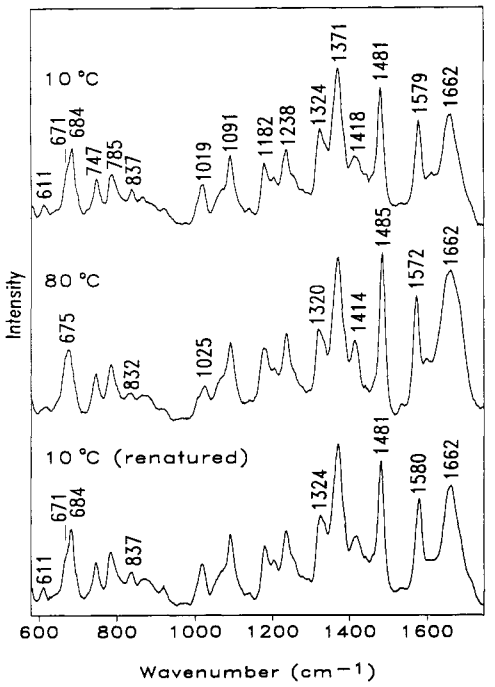

FIGURE 1: Temperature dependence of the Raman spectrum of Oxy-4, dissolved at 2 mM in 100 mM NaCl solution, pH 7.0. The initial spectrum at 10 °C (top) corresponds to the antiparallel foldback quadruplex. The middle spectrum was collected at 80 °C and represents a largely denatured structure. The bottom spectrum was obtained at 10 °C following slow cooling of the sample and is essentially identical to the initial spectrum. No smoothing of spectral data was employed.

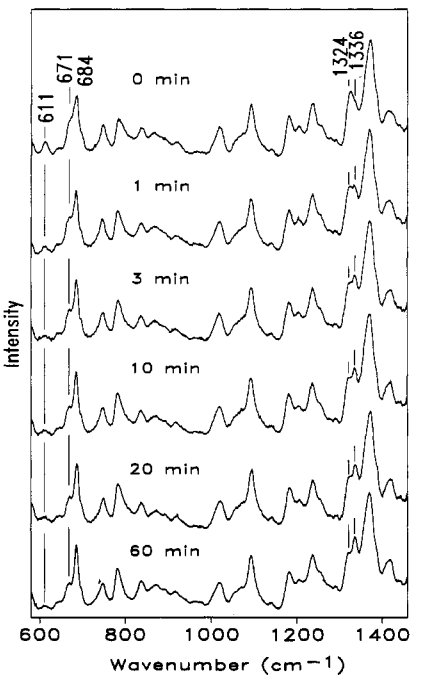

FIGURE 2: Temperature dependence of the Raman spectrum of Oxy-4, dissolved at 2 mM in 500 mM NaCl solution, pH 7.0. The initial spectrum at 10 °C (top) corresponds predominantly to the antiparallel foldback quadruplex (cf. Figure 1). The middle spectrum was collected at 80 °C after equilibration at this temperature for 60 min and represents transformation of Oxy-4 to a parallel stranded quadruplex which is retained upon cooling back to 10 °C (bottom). (See text.)

of Oxy-4 from an antiparallel foldback quadruplex containing both C2′-*endo*/*anti* and C2′-*endo*/*syn* dG to another structure containing only C2′-*endo*/*anti* dG.

d. Formation of a Parallel Stranded Quadruplex at Equilibrium in 500 mM NaCl by Oxy-4. The Raman markers of the Oxy-4 structure equilibrated in 500 mM NaCl are interpreted as those of a parallel-stranded quadruplex. The data of Figures 2 and 3 also demonstrate that the parallel stranded quadruplex, once formed by prolonged heating at 80 °C, is retained upon cooling to 10 °C (Figure 2, bottom). Therefore, unlike the antiparallel foldback quadruplex, which is denatured reversibly between 10 and 80 °C in low salt, the parallel quadruplex is thermostable over this temperature range in high salt. The Raman results on Oxy-4 are fully consistent with previous NMR studies of parallel quadruplexes (Wang & Patel, 1992; Aboul-ela et al., 1992) and show further that the parallel assembly is favored at equilibrium in high salt solutions.

We note that the residual shoulder remaining at 666 cm^{-1} in the spectrum of the fully equilibrated parallel quadruplex (Figure 2, bottom, and Figure 3 , bottom) is assigned confidently to dT residues. This is established both by model compound studies (T. Miura and G. J. Thomas, Jr., unpublished results) and a characteristic deuteration shift of the 666 cm^{-1} dT marker (below). Finally, the 836 and 1091 cm^{-1} bands of the parallel quadruplex (Figure 2, bottom) indicate that the local backbone geometry remains that of *B* DNA.

3. Qualitative and Semiquantitative Interpretation of Raman Markers in Oxy-4 Quadruplexes. Raman profiles in the interval 630–715 cm^{-1} of the Oxy-4 parallel quadruplex in H_2O and D_2O solutions are shown on an expanded scale in the left panel of Figure 4. Deuterium substitution at the thymine imino (3ND) site shifts the thymine marker from 666 to 651 cm^{-1}, consistent with data obtained on poly(dT)

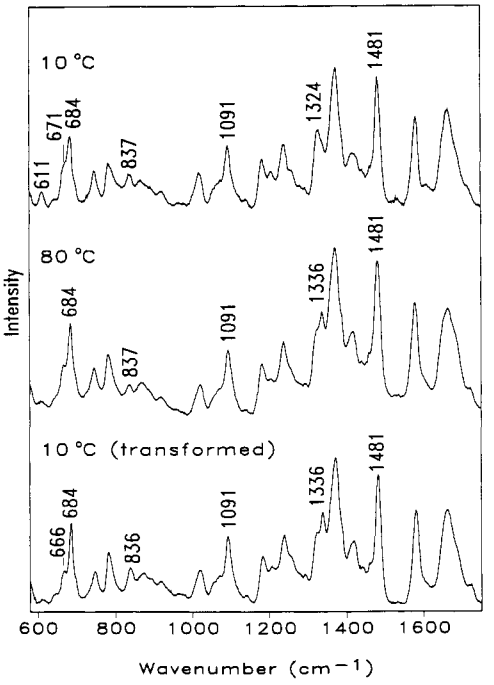

FIGURE 3: Time dependence of the Raman spectrum (580–1460 cm^{-1}) of Oxy-4 in 500 mM NaCl, equilibrated at 80 °C for the periods indicated. Data were collected at 10 °C.

(not shown). However, the C2′-*endo*/*anti* dG marker at 684 cm^{-1} is insensitive to the guanine imino (1ND) and amino ($2ND_2$) deuterations (Prescott et al., 1984). [The origin of the weak 697 cm^{-1} band is uncertain, although assignments have been proposed (Nishimura et al., 1986a).] The spectra of Figure 4a,b show conclusively that the 666 cm^{-1} band in the Oxy-4 structure is due to thymidine residues.

Figure 4c displays the Raman profile (650–715 cm^{-1}) of the Oxy-4 antiparallel quadruplex in H_2O solution. The broad

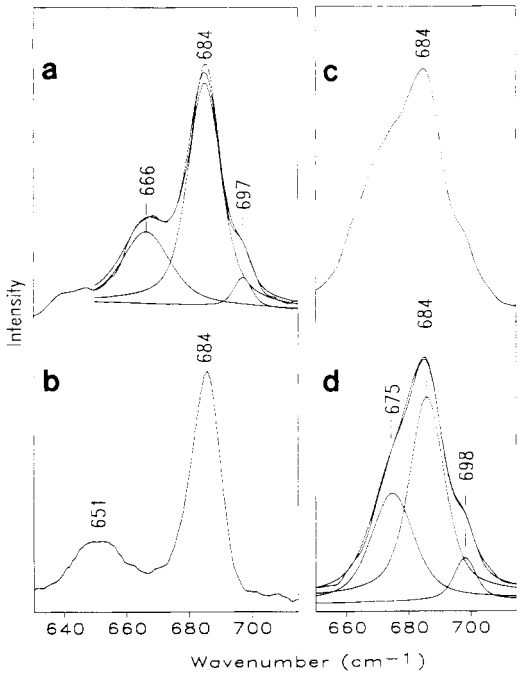

FIGURE 4: Raman spectra of Oxy-4 in the region of dG nucleoside conformation markers. (a) Experimental band profile of the parallel quadruplex in 500 mM $NaCl/H_2O$ solution (pH 7) and its fit to three Gauss–Lorentz components of the wavenumbers indicated. (b) Experimental band profile of the parallel quadruplex in 500 mM $NaCl/D_2O$ solution (pD 7). (c) Experimental band profile of the antiparallel quadruplex in 100 mM $NaCl/H_2O$ solution (pH 7). (d) A difference spectrum obtained by subtracting from c the contribution of thymine ca. 666 cm^{-1} and its fit to three Gauss–Lorentz components of the wavenumbers indicated. (The weak 697 cm^{-1} band is unassigned.)

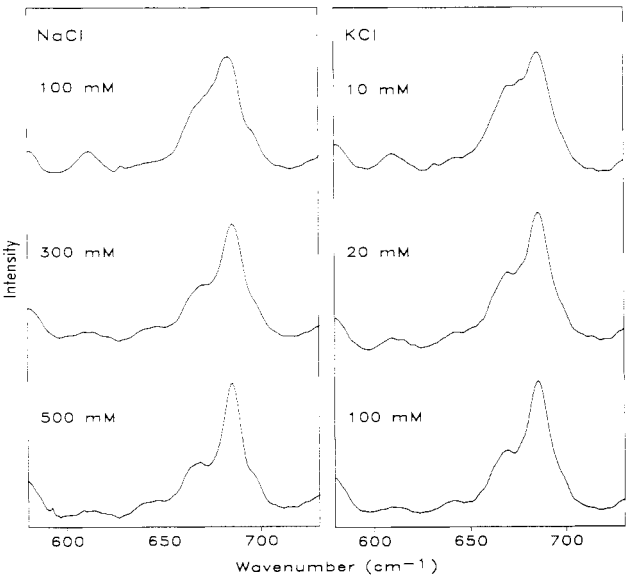

FIGURE 5: Effects of Na^+ and K^+ on Raman spectra (580–730 cm^{-1}) of Oxy-4. Left panel: Oxy-4 at 2 mM in solutions containing 100, 300, and 500 mM NaCl. Right panel: Oxy-4 at 2 mM in solutions containing 10, 20, and 100 mM KCl. Other conditions are as given in Figure 1.

and asymmetric band reflects two dG components, C2′-*endo/syn* (671 cm^{-1}) and C2′-*endo/anti* (684 cm^{-1}), as well as a dT component (666 cm^{-1}). Spectral subtraction of the latter leads to the difference profile shown in Figure 4d. Curve fitting of this complex dG band locates the C2′-*endo/syn* and C2′-*endo/anti* components at 675 and 684 cm^{-1}, respectively, close to the values inferred by simple inspection of the raw data. Several conclusions may be drawn from Figure 4.

First, our results locate the C2′-*endo/syn* dG marker at 675 ± 2 cm^{-1}. This is within experimental uncertainty of the value (671 ± 2 cm^{-1}) proposed on the basis of Raman analysis of Z DNA crystal structures (Benevides et al., 1984, 1989). Second, the simple-curve fitting analysis of Figure 4d indicates relative band intensities for the 675 and 684 cm^{-1} dG markers which are as expected if equal populations of the *syn* and *anti* conformers are present in the antiparallel quadruplex. This follows from the fact that the two dG markers have different intrinsic Raman intensities, as revealed in Z DNA, A DNA, and B DNA crystal structures (Thomas and Wang, 1988).

The present results also shed new light on conformation-sensitive Raman bands outside the 620–800 cm^{-1} region. For example, the 1324 cm^{-1} band (Figure 3) is intense in the spectrum of the antiparallel quadruplex but weak in the parallel quadruplex. This suggests that the intense 1324 cm^{-1} band is diagnostic primarily of C2′-*endo/syn* dG. A 1324 cm^{-1} marker was not detected in Z DNA crystal structures (Benevides et al., 1984, 1989), probably due to its obscuration by a nearby 1316 cm^{-1} marker associated with C3′-*endo/syn* dG.

Finally, the Raman spectrum of the antiparallel quadruplex (Figure 1) shows a weak but distinct band at 611 cm^{-1}, not reported previously. Since the band intensity diminishes significantly in the parallel quadruplex (Figure 2) and no similar band occurs in poly(dT), we assign the 611 cm^{-1} band tentatively as a marker of C2′-*endo/syn* dG. A small deuteration shift, to 607 cm^{-1}, is observed for D_2O solutions of the antiparallel quadruplex (data not shown).

4. Effects of Na^+ and K^+ on the Interquadruplex Equilibrium. Raman spectra of Oxy-4 in the structurally informative 600–700 cm^{-1} region are shown in Figure 5 for solutions containing different concentrations of Na^+ and K^+. Low concentration of either Na^+ or K^+ facilitates formation of the antiparallel quadruplex, while high cation concentration promotes formation of the parallel quadruplex (Miura et al., 1994).

However, a significant difference between the effectiveness of Na^+ and K^+ is evident. Figure 5 and additional data not shown indicate that the midpoint of interquadruplex conversion, as estimated from the Raman intensity ratio I_{675}/I_{684}, is *ca.* 20 mM for K^+, in contrast to *ca.* 240 mM for Na^+. Elsewhere we have described the dependence of the interquadruplex equilibrium upon the *ratio* of molar concentrations of the two alkali cations, $[Na^+]/[K^+]$, and proposed a phase diagram which defines the boundary between antiparallel and parallel structures over a wide range of salt concentration ratios (Miura et al., 1994).

5. Interconversion of Telomere DNA between Duplex and Quadruplex Structures. Raman spectra of $d(G_4T_4G_4)\cdot d(C_4A_4C_4)$, a model for the double-stranded region of telomere DNA, are shown in Figure 6. In 150 mM NaCl at 10 °C (top spectrum), the duplex exhibits characteristics of canonical B DNA, including the typical B form marker at 835 cm^{-1} and the expected guanine ring mode at 1489 cm^{-1}. At 80 °C, significant broadening occurs in the bands at 835 and 682 cm^{-1} (dG), and intensity increases occur in bands at 1529 (dC), 1239 (dT and dC), 783 (dC), and 729 cm^{-1} (dA). These spectral changes are reversible and indicate reversible denaturation of the B DNA duplex (Peticolas et al., 1985).

In 150 mM KCl, the spectrum of the same oligonucleotide mixture (Figure 6, bottom) exhibits distinctive differences from the corresponding spectrum in 150 mM NaCl. Notably, Raman bands at 1529, 1239, 783, and 728 cm^{-1} are more

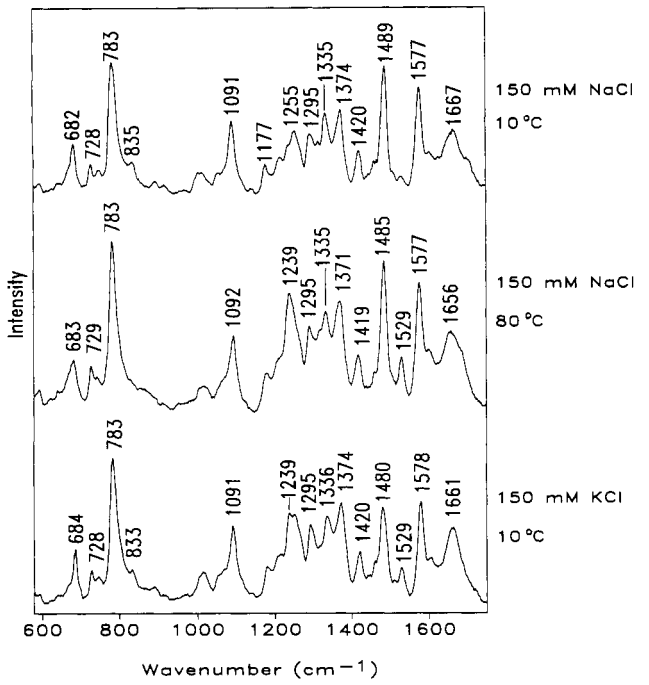

FIGURE 6: Raman spectra (580–1750 cm^{-1}) of mixtures of 2 mM $d(G_4T_4G_4)$ and 2 mM $d(C_4A_4C_4)$ at pH 7.5 in 150 mM NaCl at 10 °C (top) and 80 °C (middle) and at pH 7.5 in 150 mM KCl at 10 °C (bottom). Samples were equilibrated at 90 °C for 5 min and cooled slowly before Raman analysis. Other conditions are as given in Figure 1.

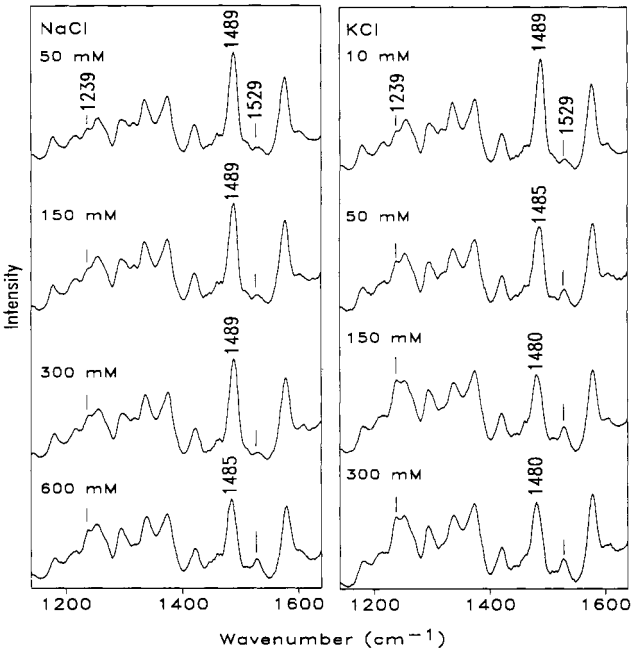

FIGURE 7: Raman spectra (1150–1640 cm^{-1}) of mixtures of 2 mM $d(G_4T_4G_4)$ and 2 mM $d(C_4A_4C_4)$ at pH 7.5 and 10 °C in solutions containing the indicated concentrations of NaCl (left panel) and KCl (right panel). Other conditions are as given in Figure 6.

intense in the K^+ environment, suggesting alteration of the *B* DNA duplex structure. Comparison with the spectrum of the thermally denatured DNA (Figure 6, middle) shows that the Raman signature of $d(G_4T_4G_4)\cdot d(C_4A_4C_4)$ equilibrated in 150 mM KCl is consistent with loss of duplex structure. The data can be rationalized by noting that the Raman bands diagnostic of dG are the same as those of the parallel-stranded quadruplex structure identified in Figure 2. We conclude that equilibration of $d(G_4T_4G_4)\cdot d(C_4A_4C_4)$ in 150 mM K^+ leads to disproportionation of the duplex and formation of a parallel-stranded quadruplex of Oxy-1.5 plus single-stranded csOxy-1.5, in accordance with eq 1. The most important

$$4[d(G_4T_4G_4)\cdot d(C_4A_4C_4)] \rightarrow [d(G_4T_4G_4)]_4 + 4[d(C_4A_4C_4)] \quad (1)$$

structural features of the Oxy-1.5 parallel quadruplex revealed in the Raman spectrum of Figure 6 (bottom) are Hoogsteen 7N hydrogen bonding (1480 cm^{-1} marker), uniformity of deoxyguanosine nucleosides in the C2′-*endo/anti* conformation (sharp 684 cm^{-1} marker), and local phosphodiester geometry similar to that of the B form backbone (833 cm^{-1} marker). (The present results do not exclude the possibility that disproportionation is also accompanied by subtle structural changes in the $d(C_4A_4C_4)$ strand.)

In a previous two-dimensional electrophoresis and chemical modification study (Lyamichev et al., 1989) it was shown that the cytosine-rich strand of *Tetrahymena* telomere DNA, $(G_4T_2)_n\cdot(A_2C_4)_n$, when inserted into a plasmid, forms a hairpin structure stabilized by hemiprotonated $C^+\cdot C$ base pairing under superhelical stress near pH 4.5. Also, previous Raman studies have demonstrated polymorphism in poly(dG)·poly(dC), involving conversion from a B form to an A form duplex in either high salt at pH 7 or in fibers at low relative humidity (Nishimura et al., 1985b, 1986b; Benevides et al., 1986). However, a quadruplex structure for guanine-rich oligo- or polydeoxynucleotides has not been reported previously. The Raman spectrum of Figure 6 (bottom) provides the first experimental evidence of a duplex-to-quadruplex conversion in a telomeric DNA model.

Raman spectra of $d(G_4T_4G_4)\cdot d(C_4A_4C_4)$ in solutions containing different concentrations of Na^+ and K^+ are shown in Figure 7. These spectra show that intensity increases in the bands at 1529 and 1239 cm^{-1} and a shift to lower frequency of the band at 1489 cm^{-1} proceed as the concentration of either salt increases. The data indicate that high ionic strength promotes the transition of $d(G_4T_4G_4)\cdot d(C_4A_4C_4)$ from duplex to parallel quadruplex in accordance with eq 1. The transition requires higher $[Na^+]$ than $[K^+]$, which is similar to the requirement for the antiparallel to parallel quadruplex transition represented in Figure 5. The midpoint of the duplex ↔ quadruplex equilibrium, estimated from the Raman intensity change at 1529 cm^{-1}, requires 550 mM Na^+ or 40 mM K^+.

DISCUSSION AND CONCLUSIONS

1. Dependence of the Polymorphism of Telomeric DNA on the Na^+ and K^+ Concentrations. It has long been observed that metal ions induce and stabilize quadruplex structures in guanine and inosine-rich nucleic acids. For example, in the quadruplex structure formed by polyinosinic acid, equilibrium dialysis studies reveal a stoichiometry of one rubidium ion for each pair of base quartets (neglecting phosphates). Howard and Miles (1982) proposed that the Rb^+ ion is situated along the central axis between quartets and is coordinated to the eight exocyclic carbonyls, consistent with metal binding at every other potential axial site. Recent X-ray analysis of the crystal structure of Oxy-1.5 (Kang et al., 1992) indicates an antiparallel foldback quadruplex structure and suggests coordination of a single ion (K^+) between the inner two guanine quartets, analogous to poly(rI)–Rb^+ coordination. On the basis of these observations and the present results, we propose a complex scheme for Oxy-4 polymorphism which is dependent upon the concentrations of *both the metal ion and DNA*, as shown in Figure 8.

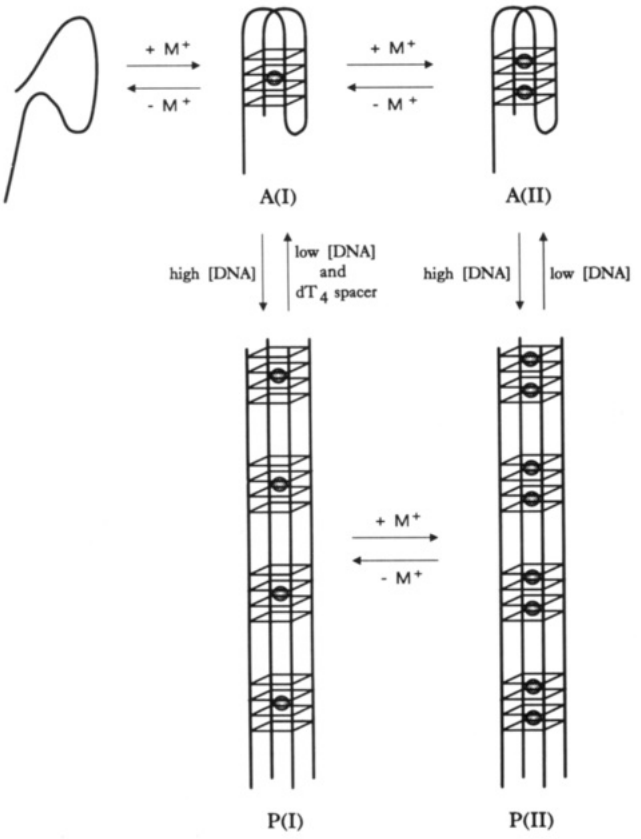

FIGURE 8: Schematic representation of Oxy-4 polymorphism, showing equilibria between the unfolded form and antiparallel foldback quadruplexes [**A(I)** and **A(II)**], above, and between parallel extended quadruplexes [**P(I)** and **P(II)**], below. High concentrations of metal ion (M^+) favor the structures at the right, while high concentrations of DNA favor the structures at the bottom.

At relatively low metal ion concentrations, the antiparallel quadruplex **A(I)** is favored by low DNA concentration and the parallel quadruplex **P(I)** is favored by high DNA concentration. Both **A(I)** and **P(I)** can be stabilized by one metal ion per Oxy-4 molecule (i.e., 1 metal per 16 guanines), provided that the metal ion concentration is relatively low. As the metal ion concentration is increased, **A(I)** and **P(I)** are converted, respectively, to the quadruplexes **A(II)** and **P(II)**, which are stabilized by two metal ions per DNA molecule (2 metals per 16 guanines). The equilibria between antiparallel and parallel quadruplexes in Figure 8, viz. **A(I)** ↔ **P(I)** and **A(II)** ↔ **P(II)**, are of course dependent upon the total DNA concentration.

Another important factor which influences the polymorphism of telomeric DNA is the length of the dT spacer between dG tracts (Balagurumoorthy et al., 1992). While Oxy-1.5 [$d(G_4T_4G_4)$] in 70 mM NaCl exhibits a circular dichroism (CD) profile characteristic of an antiparallel foldback quadruplex (peak at 295 and trough at 265 nm), this profile is attenuated as the number of dT residues in the intervening dT tract is reduced. The CD spectrum of $d(G_4T_1G_4)$ in fact shows a strong peak at 265 nm which is diagnostic of a parallel quadruplex structure. These results indicate that a dT spacer of appropriate length can contribute significantly to stabilization of the antiparallel foldback quadruplex structure. Conversely, the parallel extended quadruplex structure, which is formed by intermolecular association, may not be as highly sensitive to the length of the dT spacer.

In the present study we have examined the relationship between alkali metal ion concentration and the interquadruplex equilibrium of telomeric DNA containing a dT spacer of fixed length (dT_4), at a constant DNA concentration (2 mM oligonucleotide). We have found that at low alkali metal ion concentration the antiparallel quadruplex of Oxy-4 [**A(I)**] is strongly favored over other configurations. Indirectly, this reflects the important role of the dT_4 spacer at low salt, since shorter runs of dT would be expected to destabilize foldback loops and longer runs might facilitate formation of a larger family of foldback configurations. At high metal ion concentration, on the other hand, the effect of the dT_4 spacer is apparently diminished and the thermodynamically more stable parallel extended quadruplex [**P(II)**] (Lu et al., 1993) is favored. Figure 8 illustrates two pathways between **A(I)** and **P(II)**. These postulates are fully consistent with our experimental results.

The difference in effectiveness of sodium and potassium in inducing the parallel extended quadruplex structure can be attributed to the different affinities of these ions for the central cavity between guanine quartets. While K^+ can occupy the cavity with highly favorable interactions to eight guanine carbonyls, the smaller Na^+ ion interacts less effectively (Sundquist & Klug, 1989; Williamson et al., 1989). Accordingly, the critical ion concentration required to overcome the influence of the dT_4 spacers is apparently lower for K^+ than Na^+. In principle, it should be possible to probe directly the interactions of alkali metal ions with guanine carbonyls using Raman spectroscopy. In Oxy-4, however, the Raman spectra do not distinguish K^+ and Na^+ interactions, a consequence of the appreciable interference from dT residue carbonyls in the spectral interval of interest (1650–1750 cm^{-1}). In future Raman experiments, the relative binding affinities of K^+ and Na^+ for guanine carbonyls will be probed in oligonucleotides lacking dT.

2. Biological Significance of the Interquadruplex and Duplex–Quadruplex Conversions of Telomeric DNA. Cytological studies reveal many different types of interchromosome associations, which are characteristic of specific stages in meiotic and mitotic cell division cycles. For instance, telomeres of a linear eukaryotic chromosome are attached to termini of other chromosomes during interphase (Miller et al., 1963; Berendes & Meyer, 1968; Wagenaar, 1969). Such end-to-end association is observed also in purified chromosomal DNA (Lipps, 1980; Lipps et al., 1982) and is stabilized significantly by potassium ions (Oka and Thomas, 1987). The cation-specific stabilization and the number of telomeres participating in the association suggest that telomeres pair to form antiparallel foldback quadruplex structures. This is diagramed in Figure 9 (left).

Interestingly, the telomere–telomere associations during interphase occur between homologous chromosomes (Wagenaar, 1969). Wagenaar proposed that interphase chromosome association is a preparatory stage for the side-by-side pairing of homologous chromosomes during the meiotic prophase (synapsis). This could be the biological significance of the antiparallel foldback quadruplex structure of telomeric DNA. However, it is unlikely that telomeric DNA alone facilitates recognition between homologous chromosomes, since the telomeres of all chromosomes in a cell nucleus have the same base sequence. Recently, Sen and Gilbert (1988) hypothesized that synapsis is mediated by formation of parallel quadruplex structures not only at the telomeric regions, but also at internal guanine-rich regions of the chromosomes. The internal guanine-rich motifs, which are common in linear eukaryotic chromosomes (Behe, 1987; Wells et al., 1988), may act as distinct "fingerprints" for identification of specific homologous pairs. In this scenario, the transition of four DNA

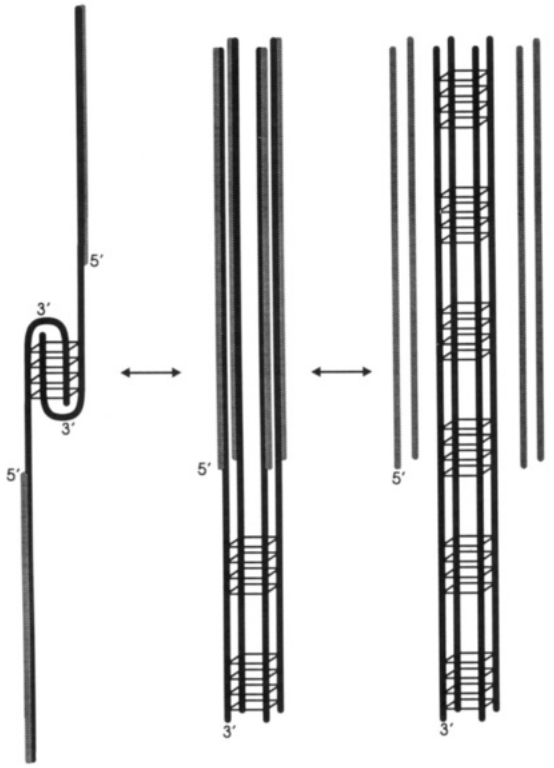

FIGURE 9: Scheme depicting possible roles of antiparallel and parallel quadruplex structures in telomeric DNA. The thick black lines represent the telomeric guanine-rich strands, and the shaded lines represent the complementary strands. During interphase, the telomeric tails of two chromosomal DNA duplexes are associated to form an antiparallel foldback quadruplex (left). At an appropriate stage in the cycle of cell division (e.g., meiotic prophase), the tails undergo a localized transition to the parallel quadruplex (middle). Subsequently, the entire telomeric DNA regions participate in the formation of an extended parallel quadruplex (right) through the duplex → quadruplex conversion.

duplexes to a parallel quadruplex at the internal guanine-rich regions is necessary for recognition and pairing of homologous chromosomes.

Three structures characteristic of telomeric DNA in cell nuclei are proposed in Figure 9. The relationship between polymorphism of telomeric DNA and interchromosome association may be summarized as follows: (i) During interphase, the single-stranded telomeric tails form an antiparallel quadruplex (Figure 9, left), which accounts for the end-to-end chromosome association. (ii) After DNA synthesis, each chromosome is present as two copies of a DNA duplex, and the antiparallel quadruplex at the telomeric tails undergoes a structural transition to a parallel quadruplex (Figure 9, middle). This transition, which is mediated by appropriate salt conditions (e.g., high K^+), results in parallel side-by-side alignment of the two pairs of sister chromatids. (iii) Finally, duplex to quadruplex structure transitions in the telomeric regions of the two pairs of sister chromatids result in formation of an extended parallel quadruplex (Figure 9, right). If interchromosome association occurs between homologous chromosomes, the internal guanine-rich regions can also form parallel quadruplex structures and tightly associate the four chromatids in zipper-like fashion. Similar side-by-side chromosome pairings may also occur during the mitotic cell cycle (summarized in Wagenaar, 1969). Mitotic associations of homologous chromosomes could be generated through the reversible antiparallel ↔ parallel interquadruplex conversions.

In the present study, we have found that the polymorphism of telomeric DNA described above can be controlled by both the *relative* and *total* concentrations of sodium and potassium ions. Although the relationship between intracellular ionic conditions and interchromosome association has not yet been explored in detail, the nuclei of living cells of the insect *Anopheles atroparvus* have been observed by phase contrast microscopy in extracellular media containing various concentrations of NaCl (Diaz & Lewis, 1975). These authors report no chromosome association at 30 mM NaCl, but parallel pairing of chromosomes at the telomeric regions with higher NaCl concentrations (≥150 mM). The chromosome associations are induced reversibly. These cytological observations are consistent with the present results; i.e., the antiparallel → parallel quadruplex and duplex → quadruplex transitions of telomeric DNA are favored by high sodium concentrations.

We have observed that both interquadruplex and duplex–quadruplex conversions are facilitated at elevated temperature (80 °C). At physiological temperature, the conversions proceed slowly because of the high thermostabilities of telomeric DNA structures. The kinetic barriers could be overcome *in vivo* by agents not included in the present *in vitro* studies, such as polyamines. For example, Howard et al. (1977) have shown that tetraethylamine significantly destabilizes quadruplex structures of poly(rG). Similar studies on telomeric DNA show that triethylamine destabilizes quadruplex assemblies and promotes structural transitions at physiological temperatures (T. Miura and G. J. Thomas, Jr., unpublished results). Cellular proteins may also play an important role in telomere polymorphism. Nevertheless, the present studies suggest that metal ion concentrations are key factors in controlling the polymorphism of telomeric DNA and that this control may extend to chromosome rearrangements which are central to meiotic and mitotic cell divisions.

ACKNOWLEDGMENT

The support of the U.S. National Institutes of Health (Grant AI18758) and Marion Merrell Dow Foundation is gratefully acknowledged. Molecular modeling was accomplished with Sybil software (Tripos Assoc., St. Louis, MO).

REFERENCES

Aboul-ela, F., Murchie, A. I. H., & Lilly, D. M. J. (1992) *Nature 360*, 280–282.

Ashley, T., & Wagenaar, E. B. (1974) *Can. J. Genet. Cytol. 16*, 61–76.

Balagurumoorthy, P., Brahmachari, S. K., Mohanty, D., Bansal, M., & Sasisekharan, V. (1992) *Nucleic Acids Res. 20*, 4061–4067.

Behe, M. J. (1987) *Biochemistry 26*, 7870–7875.

Benevides, J. M., Wang, A. H.-J., van der Marel, G. A., van Boom, J. M., Rich, A., & Thomas, G. J., Jr. (1984) *Nucleic Acids Res. 12*, 5913–5925.

Benevides, J. M., Wang, A. H.-J., Rich, A., Kyogoku, Y., van der Marel, G. A., van Boom, J. M., & Thomas, G. J., Jr. (1986) *Biochemistry 25*, 41–50.

Benevides, J. M., Wang, A. H.-J., van der Marel, G. A., van Boom, J. M., & Thomas, G. J., Jr. (1988) *Biochemistry 27*, 931–938.

Benevides, J. M., Wang, A. H.-J., van der Marel, G. A., van Boom, J. M., Rich, A., & Thomas, G. J., Jr. (1989) *Biochemistry 28*, 304–310.

Benevides, J. M., Weiss, M. A., & Thomas, G. J., Jr. (1991) *Biochemistry 30*, 5955–5963.

Berendes, H. D., & Meyer, G. F. (1968) *Chromosoma (Berlin) 25*, 184–197.

Blackburn, E. H., & J. W. Szostak, J. W. (1984) *Ann. Rev. Biochem. 53*, 163–194.

Chen, F.-M. (1992) *Biochemistry 31*, 3769–3776.
Diaz, G., & Lewis, K. R. (1975) *Chromosoma 52*, 27–35.
Erfurth, S. C., Kiser, E. J., & Peticolas, W. L. (1972) *Proc. Natl. Acad. Sci. U.S.A. 69*, 938–941.
Henderson, E. R., & Blackburn, E. H. (1989) *Mol. Cell. Biol. 9*, 345–348.
Howard, F. B., & Miles, H. T. (1982) *Biochemistry 21*, 6736–6745.
Howard, F. B., Frazier, J., & Miles, H. T. (1977) *Biopolymers 16*, 791–809.
Kang, C., Zhang, X., Ratliff, R., Moyzis, R., & Rich, A. (1992) *Nature 356*, 126–131.
Klobutcher, L. A., Swanton, M. T., Donini, P., & Prescott, D. M. (1981) *Proc. Natl. Acad. Sci. U. S. A. 78*, 3015–3019.
Lipps, H. J. (1980) *Proc. Natl. Acad. Sci. U.S.A. 77*, 4104–4107.
Lipps, H. J., Gruissem, W., & Prescott, D. M. (1982) *Proc. Natl. Acad. Sci. U.S.A. 79*, 2495–2499.
Lu, M., Guo, Q., & Kallenbach, N. R. (1993) *Biochemistry 32*, 598–601.
Lyamichev, V. I., Mirkin, S. M., Danilevskaya, O. N., Voloshin, O. N., Balatskaya, S. V., Dobrynin, V. N., Filippov, S. A., and Frank-Kamenetskii, M. D. (1989) *Nature 339*, 634–640.
Miller, O. J., Breg, W. R., Mukherjee, B. B., van Gamble, A., & Christakos, A. C. (1963) *Cytogenetics 2*, 152–167.
Miura, T., Benevides, J. M., & Thomas, G. J., Jr. (1994) submitted for publication.
Nishimura, Y., Tsuboi, M., Kato, S., & Morokuma, K. (1985a) *Bull. Chem. Soc. Jpn. 58*, 638–643.
Nishimura, Y., Torigoe, C., & Tsuboi, M. (1985b) *Biopolymers 24*, 1841–1844.
Nishimura, Y., Tsuboi, M., Sato, T., & Aoki, K. (1986a) *J. Mol. Struct. 146*, 123–153.
Nishimura, Y., Torigoe, C., & Tsuboi, M. (1986b) *Nucleic Acids Res. 14*, 2737–2747.
Oka, Y., & Thomas, C. A., Jr. (1987) *Nucleic Acids Res. 15*, 8877–8898.
Peticolas, W. L., Kubasek, W. L., Thomas, G. A., & Tsuboi, M. (1985) in *Biological Applications of Raman Spectroscopy* (Spiro, T. G., Ed.) Vol. 1, pp 81–113, Wiley, New York.
Prescott., B., Steinmetz, W., & Thomas, G. J., Jr. (1984) *Biopolymers 23*, 235–256.
Sen, D., & Gilbert, W. (1988) *Nature 334*, 364–366.
Sen, D., & Gilbert, W. (1990) *Nature 410*, 410–414.
Smith, F. W., & Feigon, J. (1992) *Nature 356*, 164–168.
Sundquist, W. I. in *Nucleic Acids and Molecular Biology* (Eckstein, F., & Lilley, D. M. J., Eds.) Vol. 5, pp 1–24, Springer-Verlag Berlin, 1991.
Sundquist, W. I., & Klug, A. (1989) *Nature 342*, 825–829.
Thomas, G. J., Jr., & Wang, A. H.-J. (1988) *Nucleic Acids Mol. Biol. 2*, 1–30.
Thomas, G. J., Jr., & Tsuboi, M. (1993) *Adv. Biophys. Chem. 3*, 1–70.
Wagenaar, E. B. (1969) *Chromosoma (Berlin) 26*, 410–426.
Wang, Y., & Patel, D. J. (1992) *Biochemistry 31*, 8112–8119.
Wells, R. D., Collier, D. A., Hanvey, J. C., Shimizu, M., & Wohlrab, F. (1988) *FASEB J. 2*, 2939–2949.
Williamson, J. R., Raghuraman, M. K., & Cech, T. R. (1989) *Cell 59*, 871–880.